

# A thermo-mechanical model of drill margin-borehole surface interface contact conditions in dry drilling of thick CFRP laminates

Yiğit Karpat<sup>a,b,c,\*</sup>, Umut Karagüzel<sup>d</sup>, Onur Bahtiyar<sup>e</sup>

<sup>a</sup> Bilkent University, Department of Industrial Engineering, Bilkent Ankara, Turkey

<sup>b</sup> Bilkent University, Department of Mechanical Engineering, Bilkent Ankara, Turkey

<sup>c</sup> UNAM – Institute of Materials Science and Nanotechnology, Turkey

<sup>d</sup> Isik University, Department of Mechanical Engineering, Sile Istanbul, Turkey

<sup>e</sup> Turkish Aerospace Industries TAI-TUSAS Kazan Ankara, Turkey

## ARTICLE INFO

### Keywords:

Drilling  
Fiber reinforced polymers  
Friction

## ABSTRACT

Dry drilling of thick carbon fiber reinforced polymer (CFRP) laminates requires careful selection of process parameters in order to obtain acceptable borehole surface quality. Complex contact conditions between the drill margin and the borehole surface determine the integrity of the borehole surface depending on the process parameters and temperature-dependent viscoelastic material properties. Temperature rise during dry drilling reduces the elastic modulus of the CFRP and causes thermal expansion of the drill, resulting in considerable contact length at the drill margin and borehole surface interface. Manufacturers need a better understanding of the interaction among contact pressure, sliding velocity, temperature at the interface, and temperature-dependent material properties to develop predictive models for drilling CFRPs. To examine this complex interaction, this study develops a novel, hybrid model that combines a time-based analytical modeling of drilling process with a finite element-based modeling of temperature rise. Drilling experiments were performed in which thrust force, torque, and temperature were measured as a function of feed, and these measurements were used to identify unknown hybrid model parameters. The results revealed that a significant change in friction conditions occurs when increased temperatures at the margin and borehole surface interface approach and exceed the glass transition temperature of the CFRP laminate at a large feed rate. These findings show the benefit of increasing feed during dry drilling, which is nonetheless limited by the temperature-dependent material properties of the work material.

## 1. Introduction

Carbon fiber reinforced plastic (CFRP) laminates offer high strength and stiffness for manufacturing the lightweight structures required in the aerospace industry [1]. When manufacturing such components, drilling many holes is required, preferably under dry conditions. The borehole quality problems caused by drilling increase the overall cost of manufacturing, as drilling is performed on readily manufactured but expensive CFRP. Therefore, the ability to predict and control process outputs during drilling of CFRPs helps to reduce component costs and improve part quality.

In dry drilling of CFRPs, its low thermal conductivity means that heat quickly accumulates at the cutting zone, which may lead to damage on the borehole surface. It is important to develop analytical and

computational models for the drilling of CFRP laminates to understand and eliminate the adverse effects of dry drilling on the machined surface. The influence of cutting temperatures on the machinability of CFRP laminates emphasizes the importance of maintaining heat balance during drilling [2]. Sadek et al. [3] developed a hybrid force and temperature model to investigate the drilling-induced delamination problem. Hintze et al. [4] showed the correlation between temperature and torque, which periodically changes depending on the fiber direction. Merino-Perez et al. [5] reported the influence of machining time on the temperature development during drilling and its possible effects on the surface quality. Wang et al. [6] showed that delamination can be reduced by controlling the temperature of the drilling environment. Fu et al. [7] investigated the drill exit temperatures while drilling UD and MD-CFRP laminates using advanced microscopy infrared thermography. They showed the close interaction between drill and CFRP work

\* Corresponding author. Bilkent University, Department of Industrial Engineering Bilkent Ankara, Turkey.

E-mail address: [ykarpat@bilkent.edu.tr](mailto:ykarpat@bilkent.edu.tr) (Y. Karpat).

<https://doi.org/10.1016/j.ijmactools.2020.103565>

Received 19 October 2019; Received in revised form 17 April 2020; Accepted 17 April 2020

Available online 23 April 2020

0890-6955/© 2020 Elsevier Ltd. All rights reserved.

Nomenclature			
$C_p$	Specific heat (J/kg.°C)	$L_{OA}$	Length of region OA on the drill (deg)
$D$	Drill diameter (mm)	$m$	Number of rotation increments
$f$	Feed (mm/rev)	$N$	Spindle rotational speed (rpm)
$f_r$	Feed rate (mm/min)	$P$	Total power (W)
$F_z$	Thrust Force (N)	$r$	Drill radius (mm)
$H$	Total drill tip height (mm)	$r_{ch}$	Chisel edge radius (mm)
$i$	Drill point location index	$t$	Time (s)
$j$	Time index	$t_{drill}$	Total drilling time (s)
$k_{11}, k_{22}, k_{33}$	Thermal conductivity (W/mK)	$w$	Web thickness (mm)
$K_c$	Force coefficient (Torque) (N/mm <sup>2</sup> )	$x, y, z$	Drill point coordinates
$K_{ch}$	Chisel edge force coefficient (N/mm <sup>2</sup> )	$T$	Temperature (°C)
$K_{ch-e}$	Chisel edge coefficient (N/mm)	$T_g$	Glass transition temperature (°C)
$K_p$	Contact force coefficient (N/mm)	$T_{g0}$	Initial glass transition temperature (°C)
$K_z$	Force coefficient (Thrust force) (N/mm <sup>2</sup> )	$T_r$	Torque (Nm)
$L$	Laminate thickness (mm)	$\beta$	Drill angle
$L_c$	Equivalent drill margin contact length (mm)	$\eta$	Heat partition to workpiece
$L_{AB}$	Length of region AB on the drill (mm)	$\mu$	Coefficient of friction at the drill margin
$L_{BC}$	Length of region BC on the drill (mm)	$\theta$	Drill tip angle
$L_{CD}$	Length of region CD on the drill (deg)	$\gamma_1, \gamma_2$	Drill angles
		$\varphi$	Drill rotation angle

material and showed that maximum temperature is reached towards the borehole exit, which hinders borehole exit quality. They also observed temperatures at the borehole exit to be larger than glass transition temperature of the CFRP. Loja et al. [8] investigated the influence of different drill types and stated that drill geometry influences temperatures, and increasing temperatures can induce damage on the workpiece. Sorentino et al. [9] measured the drill temperatures during dry drilling of both CFRP and GFRP materials. According to their results, the maximum temperature measured increased with the cutting speed and decreased with increasing feed rate. They observed decreasing temperatures in the workpiece with increasing feed rate. In a recent study, Xu and Zhang [10] investigated the heat effect on the material removal during orthogonal machining of fiber-reinforced composites using a finite element modeling technique. They focused on the influence of glass transition temperature of the FRP on the chip formation process, observing that the matrix and fibers fracture in brittle mode when the temperature is below the glass transition threshold. The material deformation behavior switches to ductile mode when the temperature exceeds glass transition temperature. They suggested that ultrasonic vibration of the drill can control the increase in temperature rise and heat accumulation.

While drilling CFRPs, it is important to keep thrust forces low to reduce likelihood of delamination at the hole exit and to control temperature rise, especially when drilling thick laminates. Turki et al. [11] showed that feed has a greater effect than cutting speed on the damage of the composite. Jia et al. [12] proposed a step drill geometry that minimizes the damage and burr formation on the workpiece for Ti/CFRP stack drilling. Kuo et al. [13] proposed a single step drilling technology for multilayer metallic-composite stacks using uncoated and coated carbide tools. Geng et al. [14] proposed using a diamond core drill rather than a twist drill to perform the drilling process. Polycrystalline diamond or diamond-coated drills are usually used in dry drilling of CFRPs due to their high thermal conductivity and wear resistance. Sharp cutting edges are recommended for easier shearing of the material. In terms of drill geometry, web thinning is usually applied to decrease the length of the drills' chisel edge in order to reduce thrust forces. The design of the drill margins is also important to reduce rubbing during drilling. Kwong et al. [15] considered the influence of the minor cutting edge of the drill on the surface integrity of drilling nickel-based superalloys. They showed that the thickness of material drag in the direction of cutting (hoop) due to ploughing increases along with increasing

interaction time between the minor cutting edge and the workpiece. They pointed out that significantly high temperatures can be generated as a combination of plastic deformation of the workpiece and friction at the tool-workpiece interface. In a subsequent study, Herbert et al. [16] showed that surface anomalies due to high feed rate drilling of nickel-based superalloys can be removed with subsequent machining processes. Such an approach may not be applicable in CFRP laminates due to their low elastic modulus. A back taper angle is common in drill designs to reduce the contact between the drill and the work material. Bonnet et al. [17] pointed out the influence of back taper angle used in drill designs on the torque measurements. Seeholzer et al. [18] reported material springback heights of 10–50  $\mu\text{m}$  depending on the machining condition in their experiments. In a recent study, the margin of the drill is modified with notches so that total contact conditions and possible heat buildup on the margin are altered [19] to improve drilling performance. In addition, helical and ultrasonic drilling have also been used [20] to alleviate the problems in dry drilling. Low frequency sinusoidal movement of the drill in feed direction may also help to alter contact conditions during drilling of thick CFRP laminates [21].

The contact conditions between the drill margin and hole surface are important in terms of heat generated during drilling. The margin of the drill rubs the machined surface over many rotations and hence creates a complex tribosystem [22,23]. Rech et al. [24] reported such a condition as a closed tribological system and stated that the coefficient of friction may change with the movement of the tool due to a thermally activated phenomenon based on material properties. In early studies on tribological behavior of polymers, Grosch [25] demonstrated the strong relationship between the viscoelastic properties of rubber and its friction against a hard substrate. Grosch found that the variation of friction with temperature correlates with the changes in rubber's material properties due to temperature. Friction was considered to have components such as adhesion and deformation. Formation and breakage of adhesion bonds and the deformation of work material at the contact spots generates heat at this interface, and the viscoelastic material properties of CFRP laminates change as a function of temperature and time [26]. Persson [27] developed a theory of rubber friction and modeled the coefficient of friction as a function of the power spectral density of a randomly rough surface, the loss modulus of rubber, its temperature, normal pressure and sliding speed. Lafaye et al. [28] investigated the apparent friction (the ratio between the tangential force and the normal load) on polymeric surfaces, showing that apparent friction calculations presented

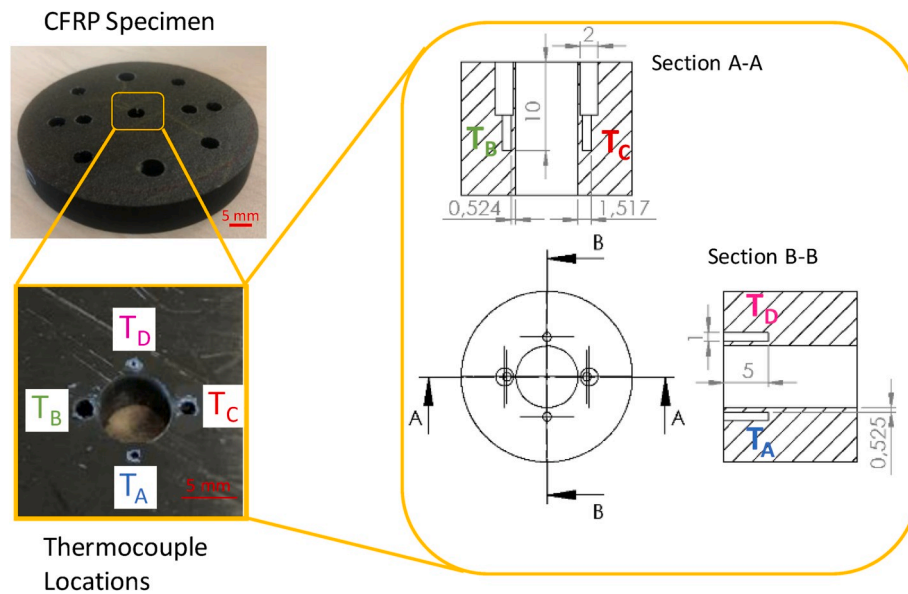


Fig. 1. CFRP specimen and placement of thermocouples at different depths (5 and 10 mm) from the top surface. The thermocouples are located 90° apart to observe the influence of fiber direction on temperature measurements.

peaks correlated with the peak loss factor (the ratio of loss to storage modulus of a viscoelastic material, which occurs at glass transition temperature of the material). Yoshizawa and Israelachvili [29] investigated adhesion friction at the molecular scale and showed that friction depends on the sliding speed due to the interpenetration of the macro-molecular chains.

To model such complex relationships, analytical and finite element based models are usually employed. A hybrid model was used in Ref. [30] to analyze surface integrity in three-dimensional turning, and a different variation was used in Ref. [31] to model the workpiece thermal distortion in the deep drilling process. Yue et al. [32] used a similar approach for the thermal modeling of electric discharge machining of CFRP. In terms of analytical modeling of drilling, mechanistic modeling is commonly used to predict thrust forces and torques as a function of drill geometry and process parameters [33,34] and it has been successfully employed in CFRP drilling as well [35,36]. In this study, a synergistic approach between mechanistic modeling and finite element modeling of temperature rise will be used to investigate the influence of contact conditions at the drill margin.

The focus of this study is on the interaction of the drill margin and the borehole surface due to the temperature rise and its effect on material properties. The intimate relationship between the drill margin and the borehole surface contact of CFRP has not been studied in detail in the literature. A time-based mechanistic model of drilling was developed to analyze the contact forces at the drill margin. A finite element model of temperature rise on the borehole surface is used to study the relationship between contact forces and the temperature-based material properties of CFRP.

The paper is organized as follows: Section 2 explains the experimental setup. In Section 3, an analytical model for drilling is presented, and experimental thrust force and torque measurements were used to identify the contact forces. Section 4 develops a finite element model to predict the temperature rise during drilling, and the temperature-dependent material behavior of CFRP is analyzed based on experimental observations. The model and the experimental findings are combined to investigate the contact conditions at the drill margin borehole surface.

## 2. Experimental setup

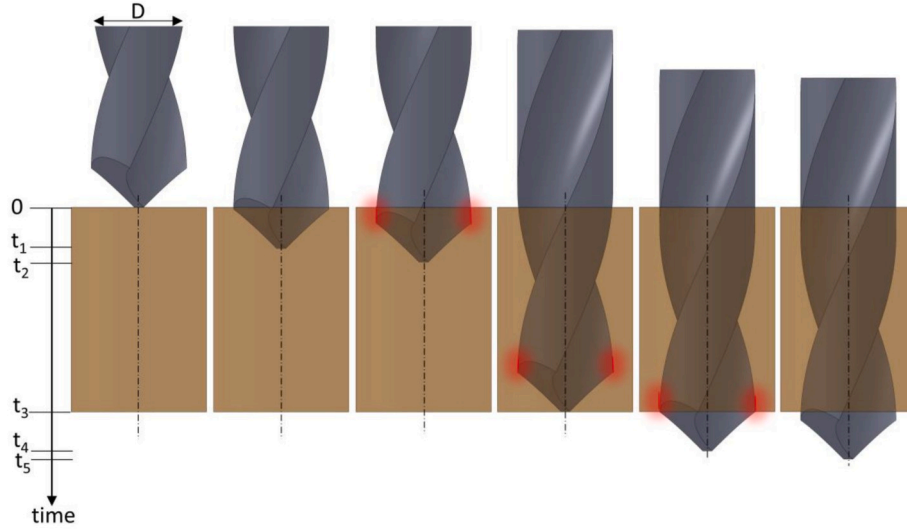
In order to investigate the drill-margin contact experimentally,

intermediate modulus UD-CFRP (CYCOM 977-2-IM7) laminates were produced for this study. The toughened epoxy resin unidirectional tape (with added rubber compounds to counteract brittleness) used in this study has 59% fiber volume with 2690 MPa tensile strength. CFRP laminate specimens of 75 mm diameter and 15 mm thickness were prepared for drilling tests. UD-CFRP laminates have 0.19 mm ply thickness and consist of 78 layers with equal fiber directions repeating in a sequence of 0/45/90/135° with two layers of 45 and 135 laminates on the top and bottom surfaces. The CFRP plate was placed on a Kistler 9275 table type dynamometer for simultaneous measurement of temperature, thrust force, and torque. Four thermocouples (K-type, -200-1200 °C range) were integrated in the CFRP laminate specimens for temperature measurements. Holes with 1 mm diameter with equal distance from the hole center were drilled and thermocouples were inserted in these holes at depths of 5 mm and 10 mm from the top surface of the laminate 90° apart from each other as shown in Fig. 1. The reason for this placement is to observe the temperature distributions on different fiber directions as well as to repeat temperature measurements. IR thermography method was used to measure temperatures at the hole exit. Another test setup was used, where the drill was attached to a robotic drilling arm and the CFRP specimen was attached to a fixture. The temperature measurements (FLIR A325SC, 0–350 °C range, 60 Hz framerate, 320x240 resolution) were conducted at various feeds. The emissivity coefficient was determined as approximately 0.85 by placing the sample into an oven as its surface temperature was monitored using both a thermocouple and an infrared camera [37]. This study used a diamond coated carbide drill (Walter Titex AF1D) with 6.96 mm diameter and a tip angle of 86°.

## 3. Analysis of contact forces at the drill-margin workpiece interface

### 3.1. Mechanistic modeling of drilling including contact forces at the drill-margin

Fig. 2(a) represents the stages of drilling from the point where the drill tip touches the work material ( $t = 0$ ) until it leaves the drilled hole ( $t = t_5$ ). Fig. 2(b) represent the three dimensional model of the drill and the forces acting on it. The contact between the drill margin and work material initiates between time points  $t_1$  and  $t_2$  and continues until the end of drilling at time point  $t_5$ . The thermal expansion of the drill and the



(a)

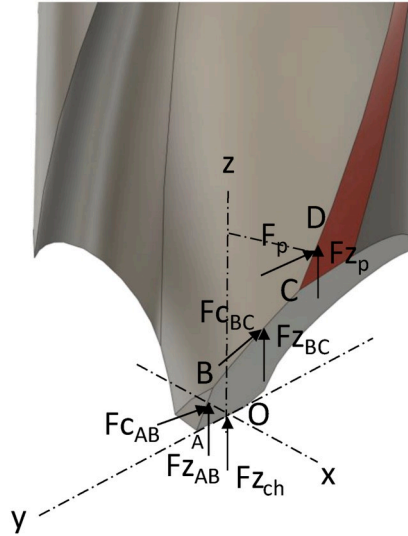


**Fig. 2.** (a) Drilling stages as a function of time (0- $t_5$ ) with drill margin-hole surface contact conditions emphasized, (b) The forces acting on a drill body are shown in the figure. The contact between the drill margin and work material initiates after time point  $t_1$ .

decreasing elastic modulus of the material with increasing temperature both affect the contact conditions between the hole wall and the drill margin. A significant decrease in the modulus of elasticity (storage modulus) of the CFRP material with increasing temperature results in increased contact area between the drill and the material.

Mechanistic modeling of drilling process is adapted from Ref. [33, 34] and the details of the time based formulation can be found in Appendix 1. The drill geometry is discretized into small elements and thrust force and torque acting on each increment ( $dl$ ) between two successive points along the cutting edge can be calculated using a mechanistic model as in Eqs. (1) and (2). The total thrust force ( $F_z$ ) and torque ( $T_r$ ) acting on the drill can be calculated by summing incremental elements using Eq. (3) and Eq. (4), respectively.

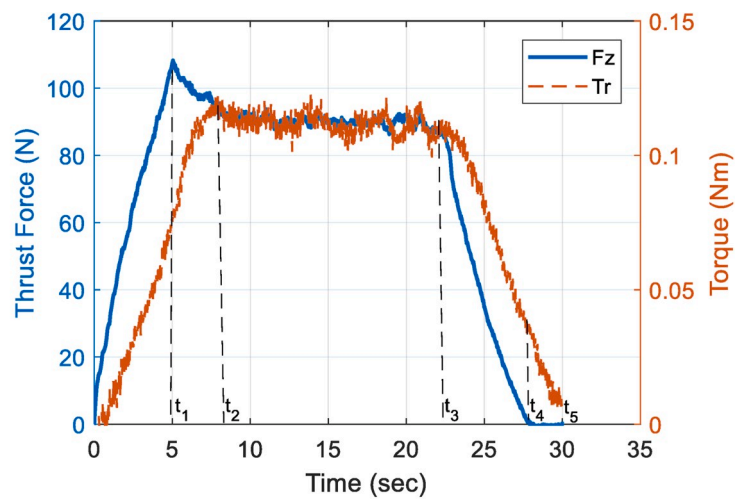
$$T_r = \begin{cases} Tr_{ij} = r_i \cdot dl_i (K_{c_j} f \sin(\theta) / 2) & AB \\ Tr_{ij} = r_i \cdot dl_i (K_{c_j} f \sin(\theta) / 2) & BC \\ Tp_{ij} = r \cdot K_{p_j} \cdot dl_i & CD \end{cases} \quad (2)$$

$$F_z = F_{z_{ch}} + 2 \sum_j \sum_i (F_{z_{ij}} + F_{z_{pij}}) \quad (3)$$

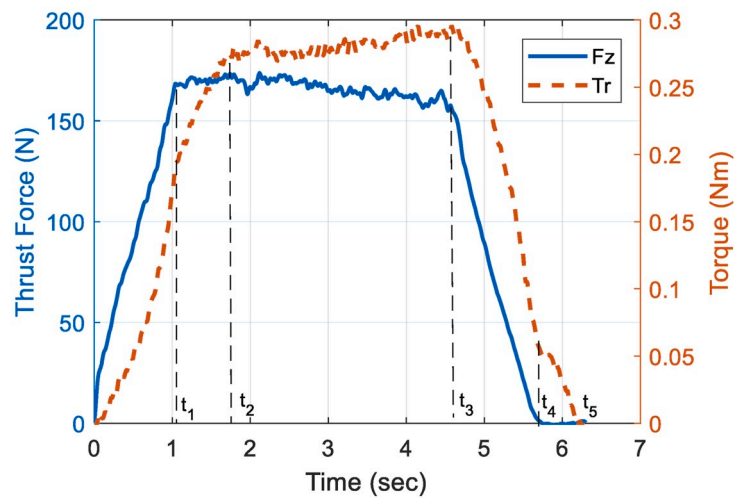
$$T_r = 2 \sum_j \sum_i (Tr_{ij} + Tp_{ij}) \quad (4)$$

The contribution of the chisel edge  $F_{z_{ch}}$  on the thrust force is defined as a function feed in Eq. (1). Force coefficients ( $K_{ch}$ ,  $K_p$ ,  $K_z$ ,  $K_c$ ) represent the materials' resistance to the machining process. The force coefficient  $K_p$  represents the influence of the drill margin workpiece interface on the torque. The contribution of drill margin region on thrust force ( $F_z$ ) depends on the friction conditions between the margin and the hole surface through an unknown apparent coefficient of friction ( $\mu$ ) [24]. The force coefficient  $K_z$  represents the influence of the main cutting edge on the direction of the tool movement. The force coefficient  $K_c$  represents the resistance of the material in the direction of tool rotation. In

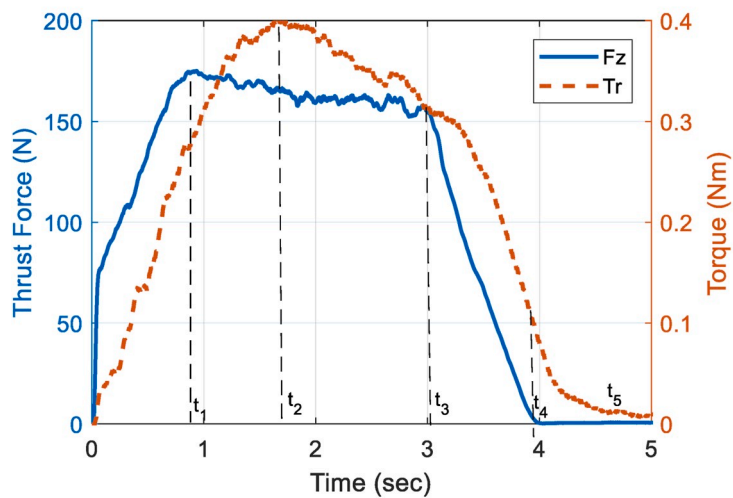
$$F_z = \begin{cases} F_{z_{ch}} = K_{ch} f + K_{ch-e} & OA \\ F_{z_{ij}} = (dl_i (K_{z_j} f \sin(\theta) / 2)) & AB \\ F_{z_{ij}} = (dl_i (K_{z_j} f \sin(\theta) / 2)) & BC \\ F_{z_{pij}} = \mu \cdot K_{p_j} \cdot dl_i & CD \end{cases} \quad (1)$$



(a)



(b)



(c)

Fig. 3. Thrust force and torque measurements for different feeds: a) 0.01 mm/rev, b) 0.05 mm/rev, c) 0.06 mm/rev. The figures show characteristic drilling stages (0-t<sub>5</sub>) for each feed.

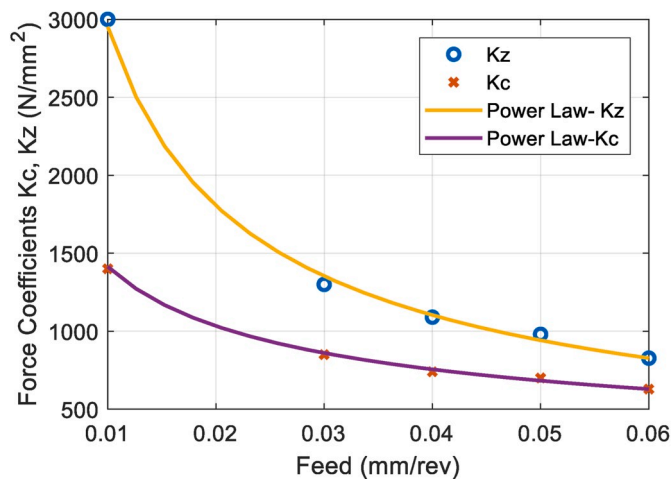


Fig. 4. Variation of force coefficients  $K_c$  and  $K_z$  calculated at time point  $t_1$  as a function of feed. Power-law equations represent a good fit for each force coefficient.

order to calculate thrust force and torques for a given feed ( $f$ ) value, unknown cutting force coefficients ( $K_{ch}$ ,  $K_p$ ,  $K_z$ ,  $K_c$ ) must be determined through drilling tests. For that purpose, drilling experiments were performed at a constant 87 m/min cutting speed ( $N = 4000$  rpm) and various feeds ( $f = 0.01, 0.03, 0.04, 0.05$ , and  $0.06$  mm/rev). Feed was increased from low to high in order to investigate the influence of sliding velocity and its influence on the temperature rise at the drill margin workpiece interface. Fig. 3(a) represents the thrust force and torque measurements for the drilling at feed of 0.01 mm/rev (feed rate of 40 mm/min). This feed was selected to be quite low, which results in increased drilling time of around 30 s. In Fig. 3(a), characteristic time points due to drill geometry during drilling can be identified as  $t_1$ - $t_5$ . From 0- $t_1$ , the drill tip enters the workpiece and the thrust force reaches its peak value at  $t_1$ . Between  $t_1$ - $t_2$ , torque continues to increase due to contact between the margin of the drill and the hole surface of the workpiece while thrust force decreases at low feed and stays stable at high feed. A similar effect can also be seen between  $t_4$  and  $t_5$  as the tool tip leaves the hole, but the contact between the margin and the hole still exists.

At  $t_3$ , the drill tip reaches the end of the hole and at  $t_4$  the drill tip leaves the hole, corresponding to zero thrust force. Between  $t_2$  and  $t_3$ , torque is stable. Stable torque measurements have been linked to the balance between temperature rise and heat removal during drilling [2]. Fig. 3(b) shows the drilling condition at 0.05 mm/rev feed. With increasing feed, both thrust force and torque increase, as expected. Thrust force has a decreasing trend towards the end of the hole. The torque slightly increases towards the end of the hole. When the feed is increased to 0.06 mm/rev, while thrust force presents a similar, decreasing trend between  $t_1$  and  $t_3$ , torque measurement switched its behavior, first rapidly increasing and then starting to decrease as shown in Fig. 3(c). Decreasing torque between  $t_2$  and  $t_3$  indicates a significant change in the contact conditions at the margin at this drilling condition. It is clear from the thrust force and torque measurements that increasing temperature during drilling changes both the material behavior and the contact conditions between the drill and work material and these changes affect the thrust force and torque measurements. The total contact length between the drill margin and the workpiece can be estimated from the torque data in the figure based on  $\Delta t$  ( $\Delta t = t_2 - t_1$ ) and feed rate. When the time difference between  $t_2$  and  $t_1$  is divided by the feed rate, the margin contact distance of around 1.8 mm for 0.01 mm/rev, 2.2 mm for 0.03 mm/rev, and 2.4 mm for 0.05 mm/rev can be calculated. These distances are significantly larger than the feed values, and therefore justify the focus of this study.

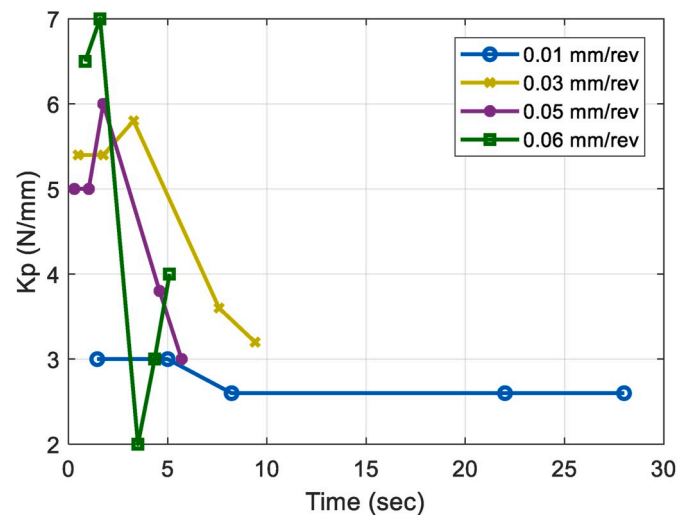


Fig. 5. Time variation of contact force coefficient  $K_p$  between  $t_1$  and  $t_5$  as a function of feed and time.

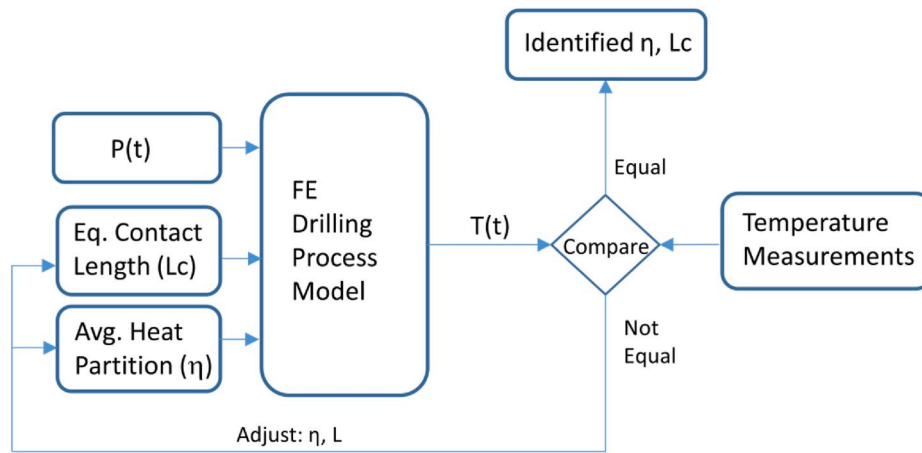
### 3.2. Identifying force coefficients through mechanistic modeling of thrust force and torque

Initial values for cutting coefficients ( $K_{ch}$ ,  $K_z$  and  $K_c$ ) can be identified considering thrust force and torque measurements at time  $t_1$  for drilling experiments performed under different feeds as reported in Ref. [36]. Identifying initial force and edge coefficients requires minimizing the difference between mechanistic model predictions and thrust force and torque measurements at time  $t_1$ . Identified force coefficients are shown in Fig. 4 as a function of feed, and they indicate the size effect while drilling CFRP laminates considering the cutting edge radius (around 10  $\mu$ m) of the drill. The linear relationship for the chisel edge force is identified as  $F_{zch} = 220f + 11.6$  and its effect is kept constant in calculations. The relationship between feed and force coefficients can be defined using a power law as.

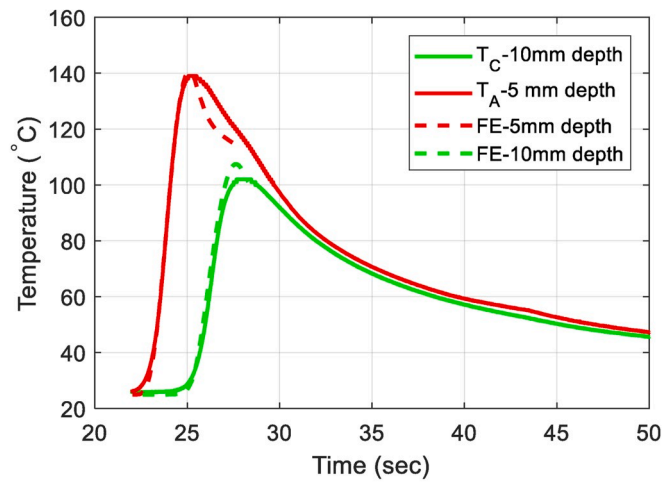
$$K_c = 176.3f^{-0.452} \text{ and } K_z = 112.23f^{-0.71}.$$

At  $t_1$ , the influence of  $K_p$  is not yet in effect. Since  $K_c$  was identified at  $t_1$ , where no contact exists at the drill margin, considering the small tip angle of the drill and low thermal conductivity of the material, it is assumed that temperature rise at the drill's main cutting edge has already increased to a certain level, and its influence is already reflected on the measured thrust force and torque. Therefore,  $K_c$  and  $K_z$  will be kept constant at their calculated values at  $t_1$  and it is assumed that the temperature rise due to contact at the drill margin during  $t_1$  and  $t_2$  will mainly affect the contact force coefficient  $K_p$ . A line contact between the margin and the hole surface is assumed for simplicity to calculate  $K_p$  in N/mm. Maegawa et al. [38] identified the coefficient of friction ( $\mu$ ) at tool workpiece interface around 0.25–0.3 during milling of CFRP laminates. Identifying an instantaneous contact force coefficient requires minimizing the difference between measurements and predictions at each time instance. Fig. 5 shows the variation of contact force coefficient  $K_p$  as a function of time for different feeds. Since the values of  $K_p$  were calculated at each time point, a piecewise linear graph was used to represent the variation with respect to time. The actual change of  $K_p$  follows a continuous function.

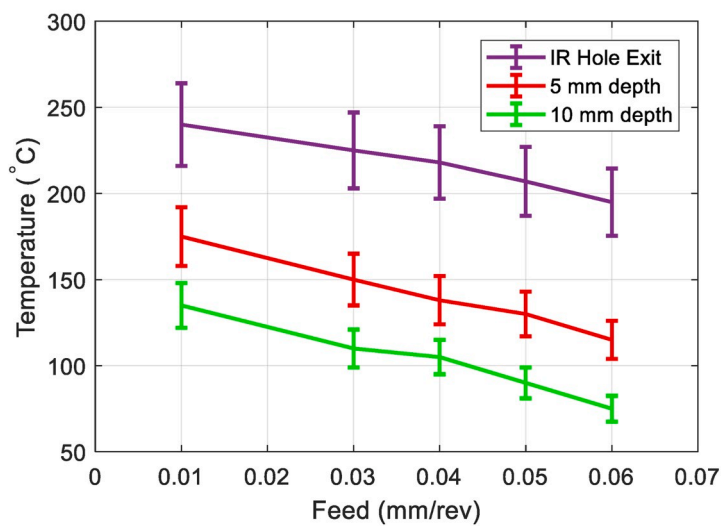
According to Fig. 5, contact force coefficients  $K_p$  tend to change their characteristic at different feeds. It has been shown that increasing temperature with increasing sliding velocity decreases the coefficient of friction, which is dependent on material properties [25]. The next section presents a finite element model based calculation of temperature rise and investigates temperature-dependent material properties.



(a)



(b)



(c)

Fig. 6. a) Parameter identification procedure used in FE model, b) Comparison of thermocouple temperature measurements and FE model temperature predictions for feed 0.03 mm/rev, c) Variation of peak temperature measurements as a function of feed including error bars representing 10% measurement uncertainty.

**Table 1**  
Results of heat partition analysis.

Feed (mm/rev)	Heat Partition to Workpiece ( $\eta$ , %)	Equivalent Contact Length ( $L_c$ , mm)
0.01	0.43	2
0.03	0.36	2.4
0.05	0.3	2.6
0.06	0.29	2.8

**4. Model based investigation of drill margin-borehole surface interface contact conditions**

**4.1. Finite element modeling of temperature rise on the hole surface during drilling**

The temperatures of CFRP laminate during the drilling process can be modeled by considering a moving heat source that translates along the z-axis to represent the drill’s advances (feed rate) through the hole. The heat flux generated at the tool-workpiece interface can be calculated from experimentally measured thrust force  $F_z(t)$  and torque  $Tr(t)$  as a function of time which can be used to calculate the total drilling power  $P(t)$ . Drilling power is used to fracture and shear the fibers, and to overcome friction at the tool-chip and tool-workpiece interfaces and to create chips (powder) while drilling CFRP. While a portion of the power is consumed to overcome friction, it will be converted into heat and removed with the chip, while the remaining portion will be transferred into the drill and to the workpiece. The percentage of the power transferred to workpiece is defined as the heat partition to workpiece ( $\eta$ ). Heat partition is known to be a function of contact conditions between the drill and the work material depending on the cutting speed, feed, underformed chip thickness, and thermal diffusivity of the materials [39,40]. However, heat partition between workpiece, chip, and drill is not known, and it may also be time-dependent as material properties of the workpiece change with increasing temperature. Unknown average heat partition to workpiece and the equivalent contact length can be identified by matching measured and simulated workpiece temperatures in reverse fashion. An average heat partition value ( $\eta$ ) and an equivalent contact length ( $L_c$ ) are estimated at the beginning and their values are adjusted iteratively until the temperature rise profiles at depths of 5 mm and 10 mm were matched experimental measurements. Temperature measurement at the hole exit obtained with an IR camera was also used to check the FE models’ predicted temperature. The details of the finite element model and temperature measurements are given in Appendix 2. Fig. 6(a) explains the parameter identification procedure. Fig. 6(b) shows the measured and predicted temperatures, which shows a good agreement for feed value of 0.03 mm/rev. Fig. 6(c) shows a decreasing trend in measured average peak temperatures with increasing feed, It must be noted that drilling time shortens as feed increases for a constant laminate thickness, which limits the maximum temperature rise [41]. A simulation takes around 60 min on a PC with Intel Core7 2.8 GHz with 16 GB RAM.

Average heat partition to workpiece ( $\eta$ ) and the equivalent contact length ( $L_c$ ) were identified as shown in Table 1. Identified heat partition to workpiece values are in good agreement with findings from the literature [24]. Heat partition to workpiece decreases with increasing feed, which indicates the positive influence of increasing feed. It also suggests that with increasing feed, the temperature gradient does not penetrate deeper into the workpiece and high temperatures are observed at the surface layer [37].

**4.2. Influence of time and temperature on viscoelastic material properties**

In order to understand the influence of temperature rise on the thermomechanical properties of the viscoelastic CFRP material considered in this study, dynamic mechanical analysis (DMA) (Mettler

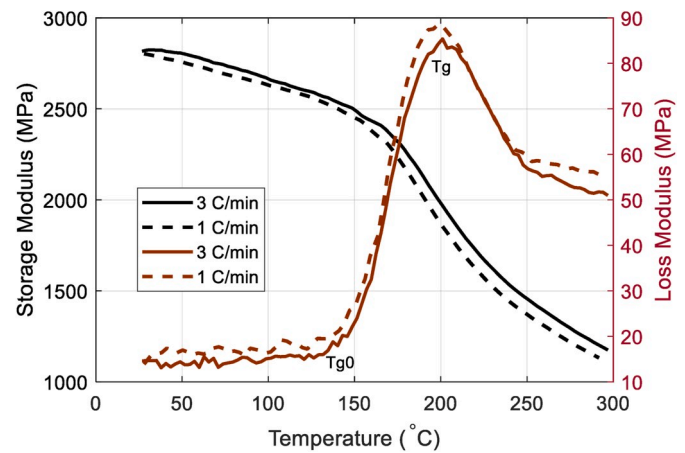


**Fig. 7.** Variation of storage and loss modulus as a function of temperature obtained via dynamic mechanical analysis performed at 1 and 3 °C/min heating rates.

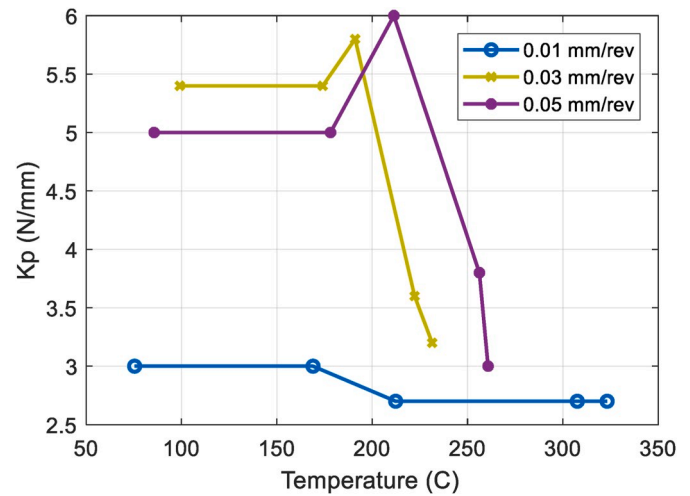


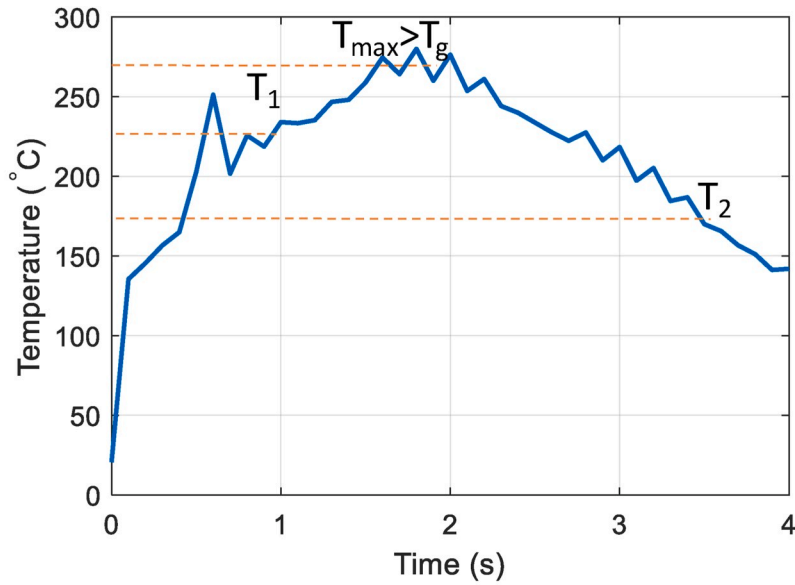
**Fig. 8.** Variation of contact force coefficient  $K_p$  as a function of feed and temperature.

Toledo–Single cantilever clamp bending test, 10- $\mu$ m amplitude, 1 Hz, from 20 to 300 °C, CFRP sample sizes of 10x15 x 3 mm, and repeated twice) was used. Fig. 7 shows the variation of storage and loss modulus as a function of temperature, and the temperature where loss modulus reaches its maximum value is named glass transition temperature ( $T_g$ ) (ASTM D4065).

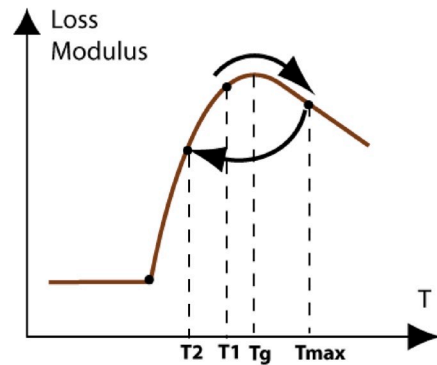
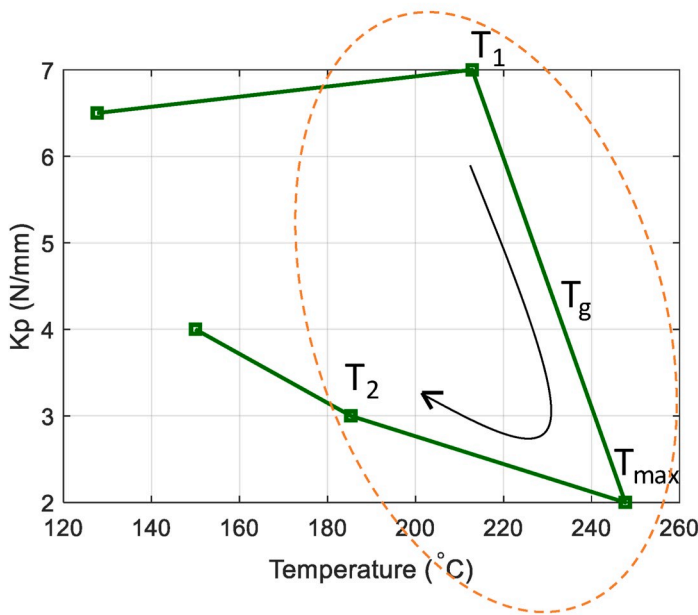
According to Fig. 7, the response of material changes significantly after 150–160 °C, which is labeled as initial glass transition temperature ( $T_{g0}$ ) on the figure. For a semi-crystalline polymer, thermal activation with increasing temperature leads to free volume between chain molecules, allowing for large-scale motions of chains that cause loss modulus to increase around glass transition temperature [42]. After this, the storage modulus starts decreasing at a higher rate, and the loss modulus starts to increase drastically before reaching its peak value at  $T_g$ , which was measured to be around 190–200 °C. The glass transition temperature is known to increase with increasing heating rate [43]. According to manufacturer’s data, glass transition temperature for this epoxy resin at 10 °C/min is 212 °C.

**4.3. Investigation of contact forces as a function of temperature at the drill margin**

We can investigate the changing material behavior due to



(a)



(b)

Fig. 9. (a) Hole surface temperature rise simulation during drilling at 0.06 mm/rev feed, (b) Variation of contact force coefficient as a function of temperature. Temperature variations are also mapped onto the loss modulus curve for visualization.

temperature rise and its influence on the contact force coefficient by combining time-based identified contact force coefficients with temperature rise data obtained from the finite element model. In Fig. 8, variation of contact force coefficient  $K_p$  (as shown Fig. 6 as a function of time) is shown as a function of temperature for feed values of 0.01, 0.03, and 0.05 mm/rev. At low feed of 0.01 mm/rev, the contact force coefficient is stable and decreases with increasing temperature. Contact force coefficients at 0.03 and 0.05 mm/rev were calculated to be close. The variation in contact force coefficients resembles the loss modulus of the material shown in Fig. 7. These findings agree with the results in Grosh, where the master curve of coefficient of friction for rubber material was correlated with the loss modulus of the material [25]. Persson

[44] showed that friction can be significantly lower with increasing temperature because of the formation of localized hot junctions at the interface between macroscopic asperities of the hard surface and the material. With increasing feed rate, the peak value of the contact force coefficient seem to shift to the right, which is also in agreement with the master curve data shown in Fig. 7. According to finite element simulation of temperature rise, heating rate ( $dT/dt$ ) can be calculated between  $t_1$  and  $t_2$ , as full contact is obtained at the margin. Between  $t_1$  and  $t_2$ , at 10  $\mu\text{m}/\text{rev}$  the heating rate was calculated as 24  $^\circ\text{C}/\text{s}$  and 70  $^\circ\text{C}/\text{s}$  at 50  $\mu\text{m}/\text{rev}$ . These heating rates are considerably higher than those heating rates (3, 10  $^\circ\text{C}/\text{min}$ ) used in DMA; therefore, higher  $T_{g0}$  and  $T_g$  values may be expected at high feed cases compared to those measured at lower

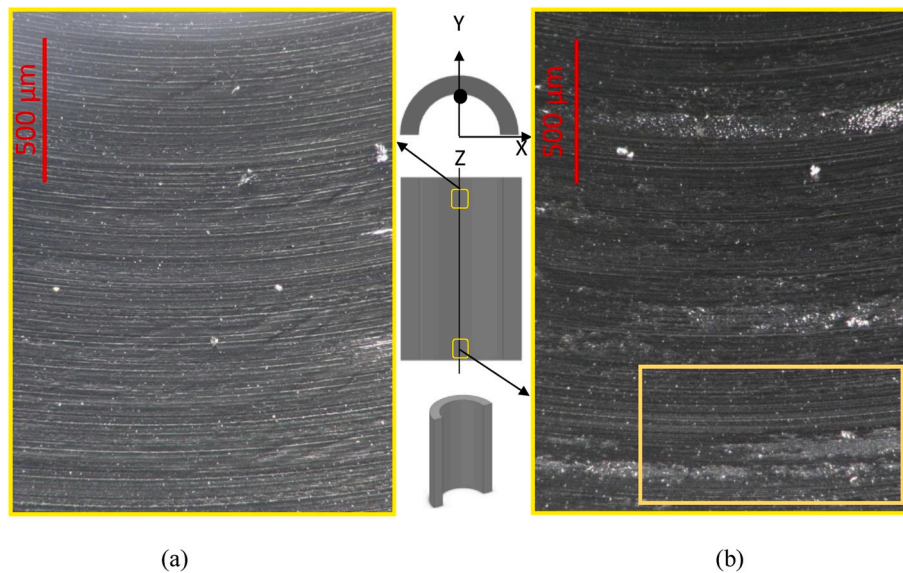


Fig. 10. a) Hole surface at the entry and b) exit corresponding to 0.01 mm/rev. Hole quality deteriorates from hole entry to hole exit.

heating rates.

Increasing loss modulus with increasing temperature result in a larger coefficient of friction at the interface [24,25]. If the temperature at the interface exceeds the glass transition temperature, changes in the crystalline structure (degree of crystallinity due to cross-linking) of the material produce the opposite effect, which leads to changing friction conditions and a decrease in contact pressure [44].

At 0.06 mm/rev feed, a situation different from those in other drilling cases occurs, where the contact force coefficient first increases and then decreases then slightly increase again as first shown in Fig. 5. Fig. 9 (a) shows the variation of temperatures obtained from FE model for 0.06 mm/rev feed.

A decrease in temperature towards the end indicates a reverse trend that was not observed in other feeds. After reaching its peak value around 260 °C (indicated as  $T_{max}$  in Fig. 9(a)) the temperature significantly drops. This lowering temperature is due to a significant decrease in measured torque during drilling (Fig. 3(c)) since it is an input to FE model. This may be due to changing frictional conditions at the drill margin interface; since a larger chip load is considered at this feed together with larger sliding velocity and higher temperature, it is possible that chips in the form of powder may have accumulated at the drill margin. Changing contact conditions would decrease the amount of heat transferred into the workpiece, resulting in lower temperatures, which in turn may end up increasing the contact forces described in Fig. 9(b). In a recent study, Waddad et al. [45] showed that debris at the interface significantly affects the heat transfer conditions and heat partition ratio during sliding contact of rough surfaces.

The mechanisms of friction are due to interfacial adhesion and ploughing or deformation. Adhesion usually originates at smooth surfaces, while deformation is due to the contact of asperities on rough or deformed surfaces [25]. In drilling, the drill margin rubs the same borehole surface over and over. Therefore, it is possible that deformations on the surface may affect the friction mechanism. The next section investigates the hole wall surfaces.

#### 4.4. Investigating the drill margin-borehole surface integrity

Fig. 10 shows the borehole surface investigation performed inside the hole for the CFRP specimens for 0.01 mm/rev. The microscope was tilted 30° and a series of surface images were collected along the hole. Fig. 10(a) shows the entry region of the hole with no defects. Fig. 10(b) shows the hole exit surface where smearing of the matrix is visible. The

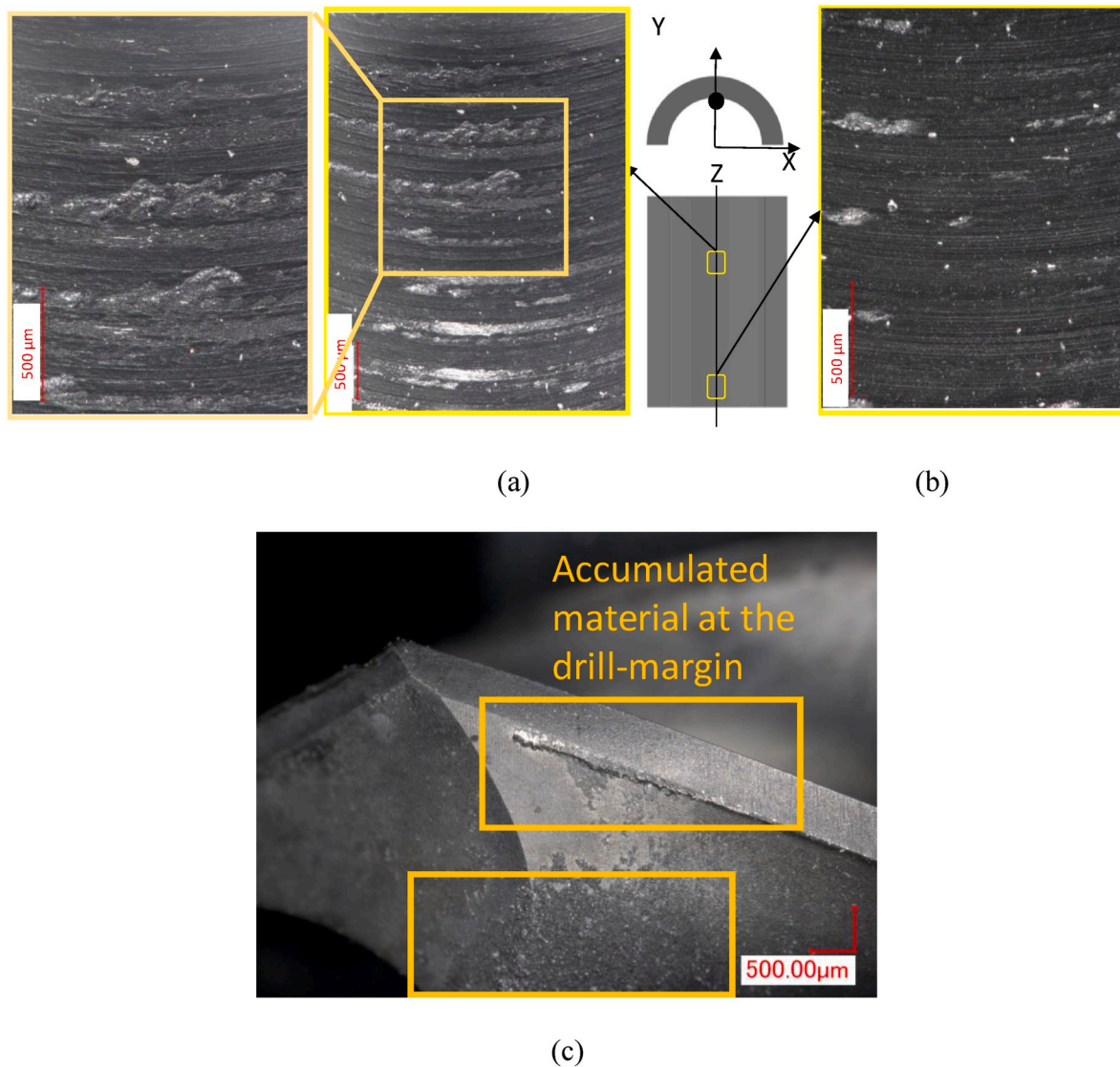
detrimental effect of slow feed drilling can therefore be seen towards the hole exit corresponding to high temperatures at that region. The surface of the hole wall is in good condition until the end of the drilled hole. This may also explain the variation of steady contact force at the interface as shown in Fig. 8.

Fig. 11(a) shows the hole surface corresponding to peak temperature location at the highest feed of 0.06 mm/rev (feed rate of 240 mm/min). Smearing of matrix and fiber pull-out defects are visible where the matrix was exposed to high temperatures. Fig. 11(b) shows the same area at the hole exit where only debris and deposited materials are visible on the drilled surface. While some defects are visible, they are not severe due to lower temperature and lower contact forces. Fig. 11 (c) shows the material adhesion on the flank of the drill margin. Debris accumulated at the drill margin may be due to loose particles at the interface or cut powdered chips smeared on the drill surface as shown in the figure. Their influence increases the complexity of the contact conditions. The deformed surface on the wall indicates the influence of large contact forces as discussed in the previous section.

While peak temperatures were observed to be larger than  $T_g$ , no sign of pyrolysis was observed, which is in line with the observations in Ref. [46]. The increase in feed is limited by the thrust forces at the hole exit, which may lead to delamination at the hole exit. No hole exit delamination problems were observed after drilling experiments. The hole diameter, which is another quality consideration, is also affected by temperature variations during drilling.

## 5. Conclusions

This paper has analyzed the problem of complex contact at the drill margin-borehole surface interface during dry drilling of CFRP laminates by considering its temperature-dependent material properties. The rise in temperature during dry drilling reduces the elastic modulus of the CFRP and causes thermal expansion of the drill, resulting in considerable contact length at the drill margin and borehole surface interface. The borehole surface integrity depends on the contact conditions at the interface. This study proposes an instantaneous mechanistic model coupled with a finite element model that predicts temperature rise on the borehole surface in order to investigate the time and temperature-dependent variation of the contact force coefficient. The results suggest that the viscoelastic properties of the work material influence its frictional behavior.



**Fig. 11.** (a) Hole surface corresponding to maximum torque location at 0.06 mm/rev together with close-up image of the damaged area, b) Hole surface towards hole exit, c) Material adhesion on the margin of the drill at feed of 0.06 mm/rev.

- Temperature-dependent material properties play a key role in determining contact conditions at the drill margin and hole surface interface. Selection of feed affects the heating rate as well as the total contact time between the drill margin and the hole wall surface. Glass transition temperature range ( $T_{g0}$  and  $T_g$ ) shifts depending on the heating rate. If the rise in temperature at the interface exceeds peak glass transition temperature and is accompanied by high contact forces, surface damage is likely to appear.
- The heating rate and consequent temperature rise seem to govern the development of thrust force and torque during dry drilling. Therefore, monitoring of thrust force and torque can be used to identify the influence of temperature rise on the hole wall surface integrity considering temperature-dependent material properties.
- These findings suggest that using low feed is not beneficial in dry drilling of thick laminates. While low feed helps to decrease thrust forces at the hole exit, the temperature rise due to inefficient cutting of the material becomes significant. Increasing feed relative to the cutting edge radius helps decrease force coefficients and transfer more heat to the chip and the drill. Meanwhile, the upper limit of the feed rate depends on chip evacuation conditions and contact conditions at the drill margin.

- It is desirable to keep temperatures lower than 160 °C to better predict process outputs by considering advanced drilling techniques such as ultrasonic drilling or low frequency sinusoidal movement of the drill. These techniques would change the contact length and limit temperature rise at the interface during drilling.

#### Funding

This research did not receive any specific grant from funding agencies in the public, commercial, or not-for-profit sectors.

#### Declaration of competing interest

None.

#### CRediT authorship contribution statement

**Yigit Karpat:** Conceptualization, Methodology, Software, Supervision, Writing - original draft, Formal analysis, Visualization. **Umut Karagüzel:** Investigation, Data curation, Writing - review & editing, Visualization. **Onur Bahtiyar:** Investigation.

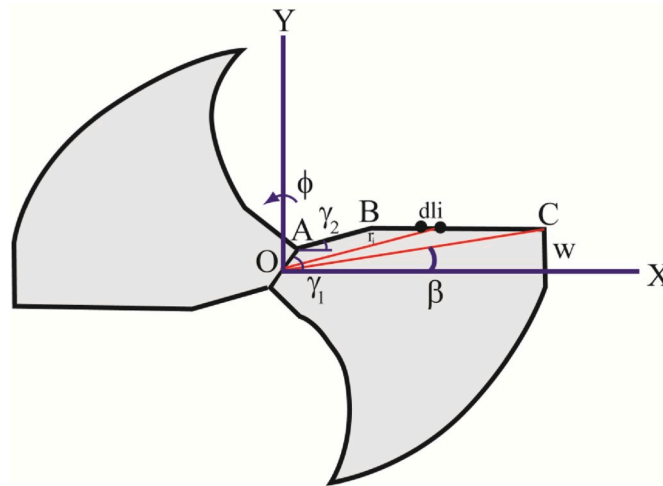
**Acknowledgments**

Technical University and Dr. L. Taner Tunç of Sabancı University Composite Research Center for their contributions to this study.

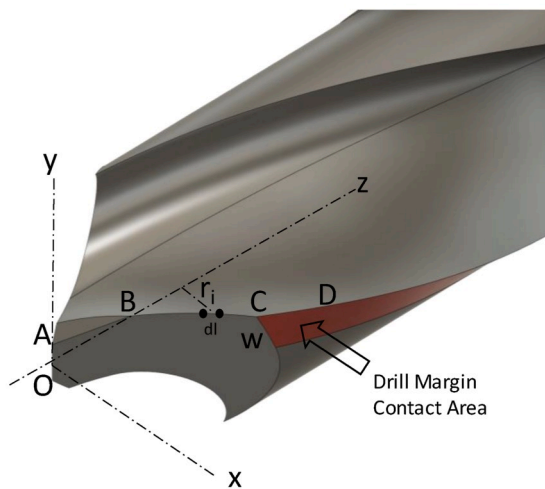
The authors would like to thank Prof. Mustafa Bakkal of Istanbul

**Appendix 1**

Fig. A1(a) shows the geometry of the drill used in this study, where OA represents the chisel edge region ( $r_{ch} = 0.175$  mm and  $\gamma_1 = 55^\circ$ ), AB shows the web thinned region ( $L_{AB} = 1$  mm,  $\gamma_2 = 15^\circ$ ), and BC shows the primary drilling region ( $L_{BC} = 2.25$  mm). Fig. A1(b) shows the drill margin contact region CD. Let us assume that the index  $i$  represents a point on the drill while the index  $j$  represents the rotation increment ( $\phi_j$ ) of the drill around its center point O as shown in Fig. A2. In Eq (A1),  $m$  represents the number of rotation increments and  $i$  depends on the number of vertical elements ( $n$ ) and the total height ( $H$ ) of the tool tip ( $H=H_{OC} + H_{CD}$ ); and  $j$  depends on the thickness of the laminate ( $L$ ) and feed ( $f$ ,  $\mu\text{m}/\text{rev}$ ). Tip height of the drill ( $H_{OC}$ ) can be calculated from the tip angle ( $2\theta = 86^\circ$ ) and the diameter ( $D$ ) of the drill. Total drilling ( $t_{drill}$ ) time for a given laminate thickness ( $L$ ) can also be calculated based on this information. The three-dimensional position of any point along the drill edge (O to C) based on drill angles can be calculated using the equations given in Table A1.



(a)



(b)

**Fig. A1.** (a) Schematic model of the drill design, b) Drill margin contact zone CD indicated on the drill. Forces acting on the drill.

$$i = H/n$$

$$j = \frac{(L + H) \cdot m}{f} \tag{A1}$$

**Table A1**  
Location calculation of points on the drill edge.

Chisel Edge (OA)	Web Thinned Edge (AB)	Primary Drilling Edge (BC)
$x = r_{ch} \cos \gamma_1$ $y = r_{ch} \sin \gamma_1$ $z = 0$ $\beta_i = \gamma_1$	$x_i = (z_i - z_{i-1}) \tan \theta + x_{i-1}$ $y_i = ((z_i - z_{i-1}) \tan \theta) \tan \gamma_2 + y_{i-1}$ $z_i = z_i$ $\beta_i = a \tan \left( \frac{y_i}{x_i} \right)$	$x_i = (z_i - z_{i-1}) \tan \theta + x_{i-1}$ $y_i = r_{ch} \sin \gamma_1 + L_{AB} \sin \gamma_2$ $z_i = z_i$ $\beta_i = a \sin \left( \frac{w}{r_i} \right)$

The trajectory of each point on the drill edge ( $x_i, y_i, z_i$ ) at a given time increment during drill's rotational movement can be calculated with Eq (A2) [33].

$$x_{i,j} = r_i \cos(\beta_i + \varnothing_j)$$

$$y_{i,j} = r_i \sin(\beta_i + \varnothing_j)$$

$$z_{i,j} = z_i - \left( \frac{L + H}{\Delta \varnothing} \right) j \quad (A2)$$

The positive direction of  $z$  is defined as the direction of drill movement, and the workpiece top surface is defined as the origin. At each point on the drill geometry, effective rake and clearance angles can be calculated [34]. By tracking a point on the drill with its  $x, y, z$  coordinates, it is possible to identify whether that point on the drill is in the cut or not. As a result, entry and exit transition zones can be obtained as a function of time.

## Appendix 2. Finite Element Model and Temperature Measurements

The heat flux generated at the tool-workpiece interface can be calculated from experimentally measured thrust force  $F_z(t)$  and torque  $Tr(t)$  as a function of time which can be used to calculate the total drilling power  $P(t)$  as shown in Eq. A2.

$$P(t) = F_z(t)fN + Tr(t)N \frac{2\pi}{60} \quad (A2)$$

The contact area between the drill margin and the hole surface can be calculated considering the periphery of the drill and contact length of the heat source. The lumped effect of workpiece heating  $q(t)$  based on these measurements of thrust force and torque as a function of time together with contact length can be calculated as  $W/m^2$ . In FE model, a moving heat source represents the equivalent thermal loading of both tool and chip on the workpiece. The layered structure of the CFRP laminate, which consists of repeating  $0^\circ, 45^\circ, 90^\circ$ , and  $135^\circ$  layers is modeled in Comsol Multiphysics software. The temperature-dependent heat capacity  $C_p$  ( $C_p(T) = 0.0029T - 0.0817(J/kg \text{ } ^\circ C)$ ) and thermal conductivities ( $k$ ) in different fiber directions ( $k_{11}(T) = 0.013T + 2.95, k_{22}(T) = 0.07T + 1.5, k_{33}(T) = 0.0007T + 0.5744 W/mK$ ) were adapted from the literature [47]. Fig. A2(a) shows the thermocouple temperature measurements obtained at  $30 \mu m/rev$  feed case. While there are some slight differences between sensors, temperature measurements were consistent within 10% error margin. Fig. A2(b) shows the thermocouple measurements for  $60 \mu m/rev$  feed drilling. Fig. A2(c) shows that temperatures measured with the IR camera at the hole exit correspond to time points  $t_3-t_5$  when the drill tip is out of cut. Each temperature measurement experiment was repeated twice. Temperature measurements are dependent on thermocouple placement with respect to fiber directions, which is a characteristic of unidirectional CFRP drilling as also observed in Refs. [4,7].

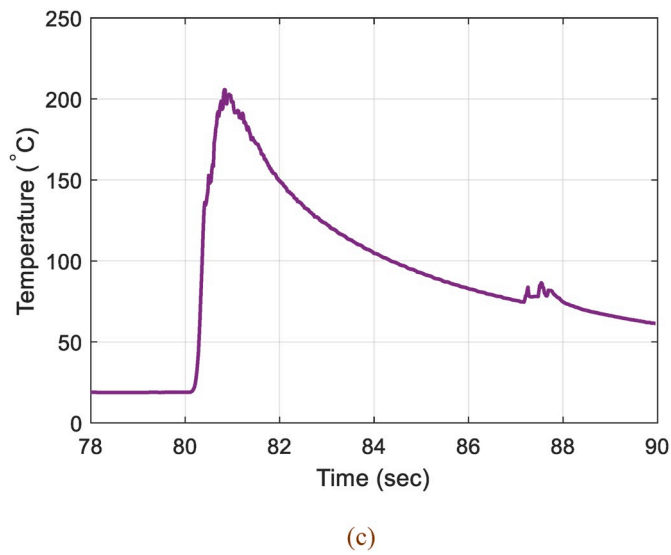
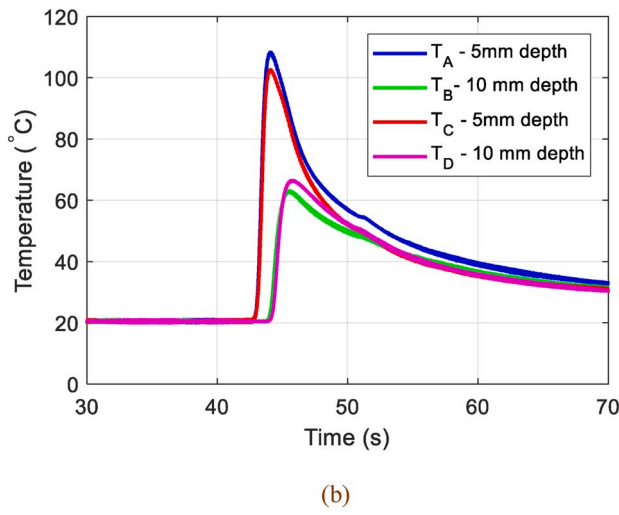
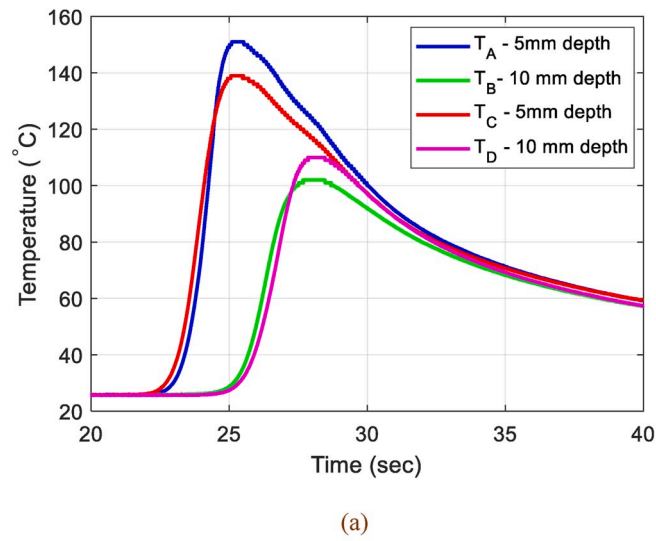


Fig. A2. Thermocouple temperature measurements for: (a) 0.03 mm/rev feed, b) 0.06 mm/rev feed, c) IR camera measurements for 0.06 mm/rev at the hole exit,

## References

- [1] J. Fleischer, R. Teti, G. Lanza, P. Mativenga, H.C. Möhring, A. Caggiano, Composite materials parts manufacturing, *CIRP Annals* 67 (2018) 603–626.
- [2] K. Weinert, C. Kempmann, Cutting temperatures and their effects on the machining behaviour in drilling reinforced plastic composites, *Adv. Eng. Mater.* 6 (8) (2004) 684–689.
- [3] A. Sadek, B. Shi, M. Meshreki, J. Duquesne, M.H. Attia, Prediction and control of drilling-induced damage in fibre-reinforced polymers using a new hybrid force and temperature modelling approach, *CIRP Annals* 64 (2015) 89–92.
- [4] W. Hintze, C. Schütte, S. Steinbach, Influence of the fiber cutting angle on workpiece temperature in drilling of unidirectional CFRP, *Lecture Notes in Production Engineering, New Production Technologies in Aerospace Industry* (2013) 137–143.
- [5] J.L. Merino-Pérez, R. Royer, S. Ayvar-Soberanis, E. Merson, A. Hodzic, On the temperatures developed in CFRP drilling using uncoated WC-Co tools Part I: workpiece constituents, cutting Speed and heat dissipation, *Compos. Struct.* 123 (2015) 161–168.
- [6] H. Wang, X. Zhang, Y. Duan, Effects of drilling area temperature on drilling of carbon fiber reinforced polymer composites due to temperature-dependent properties, *Int. J. Adv. Manuf. Technol.* 96 (2018) 2943–2951, 2018.
- [7] R. Fu, Z. Jia, F. Wang, Y. Jin, D. Sun, L. Yang, De Cheng, Drill-exit temperature characteristics in drilling of UD and MD CFRP composites based on infrared thermography, *Int. J. Mach. Tool Manufact.* 135 (2018) 24–37.
- [8] M.A.R. Loja, M.S.F. Alvesa, M.F. Bragança, R.S.B. Rosa, C.J. Barbosa, J.I. Barbosa, An assessment of thermally influenced and delamination-induced regions by composites drilling, *Compos. Struct.* 202 (2018) 413–423.
- [9] L. Sorrentino, S. Turchetta, C. Bellini, In process monitoring of cutting temperature during the drilling of FRP laminate, *Compos. Struct.* 168 (2017) 549–561.
- [10] W. Xu, L. Zhang, Heat effect on the material removal in the machining of fibre-reinforced polymer composites, *Int. J. Mach. Tool Manufact.* 140 (2019) 1–11.
- [11] Y. Turki, M. Habak, R. Velasco, Z. Aboura, K. Khellil, P. Vantomme, Experimental investigation of drilling damage and stitching effects on the mechanical behavior of carbon/epoxy composites, *Int. J. Mach. Tool Manufact.* 87 (2014) 61–72.
- [12] Z.Y. Jia, C. Zhang, F.J. Wang, R. Fu, C. Chen, An investigation of the effects of step drill geometry on drilling induced delamination and burr of Ti/CFRP stacks, *Compos. Struct.* 235 (2020) 111786, 2020.
- [13] C.L. Kuo, S.L. Soo, D.K. Aspinwall, C. Carr, S. Bradley, R. M'Saoubi, W. Leahy, Development of single step drilling technology for multilayer metallic-composite stacks using uncoated and PVD coated carbide tools, *J. Manuf. Process.* 31 (2018) 286–300.
- [14] D. Geng, Z. Lu, G. Yao, J. Liu, Z. Li, D. Zhang, Cutting temperature and resulting influence on machining performance in rotary ultrasonic elliptical machining of thick CFRP, *Int. J. Mach. Tool Manufact.* 123 (2017) 160–170.
- [15] J. Kwong, D.A. Axinte, P.J. Withers, M.C. Hardy, Minor cutting edge-workpiece interactions in drilling of an advanced nickel-based superalloy, *Int. J. Mach. Tool Manufact.* 49 (2009) 645–658.
- [16] C.R.J. Herbert, J. Kwong, M.C. Kong, D.A. Axinte, M.C. Hardy, P.J. Withers, An evaluation of the evolution of workpiece surface integrity in hole making operations for a nickel-based superalloy, *J. Mater. Process. Technol.* 212 (2012) 1723–1730.
- [17] C. Bonnet, C. G. Poulachon, J. Rech, Y. Girard, J.P. Costes, CFRP drilling: fundamental study of local feed force and consequences on hole exit damage, *Int. J. Mach. Tool Manufact.* 94 (2015) 57–64.
- [18] L. Seeholzer, R. Voss, F. Grossenbacher, F. Kuster, F. Wegener, Fundamental analysis of the cutting edge micro-geometry in orthogonal machining of unidirectional carbon fiber reinforced plastics (CFRP), 8<sup>th</sup> CIRP Conference of High Performance Cutting (HPC), *Procedia CIRP* 77 (2018) 379–382.
- [19] Z. Jian, R. Fu, B. Niu, B. Qian, Y. Bai, F. Wang, Novel drill structure for damage reduction in drilling CFRP composites, *Int. J. Mach. Tool Manufact.* 110 (2016) 55–65.
- [20] J. Liu, G. Chen, C. Ji, X. Qin, H. Li, C. Ren, An investigation of workpiece temperature variation of helical milling for carbon fiber reinforced plastics (CFRP), *Int. J. Mach. Tool Manufact.* 86 (2014) 89–103.
- [21] O. Pecat, E. Brinksmeier, Tool wear analyses in low frequency vibration assisted drilling of CFRP/Ti6Al4V stack material, *Procedia CIRP* 14 (2014) 142–147.
- [22] W. Grzesik, J. Rech, Development of tribo-testers for predicting metal cutting friction, *Journal of Machine Engineering* 19 (1) (2019) 62–70.
- [23] S.N. Melkote, W. Grzesik, J. Outeiro, J. Rech, V. Schulze, H. Attia, P.J. Arrazola, R. M'Saoubi, C. Saldana, Advances in material and friction data for modelling of metal machining, *CIRP Annals* 66 (2017) 731–754.
- [24] J. Rech, P.J. Arrazola, C. Claudin, C. Courbon, F. Pusavec, J. Kopac, Characterisation of friction and heat partition coefficients at the tool-work material interface in cutting, *CIRP Annals* 62 (1) (2013) 79–82.
- [25] K.A. Grosch, The relation between the friction and visco-elastic properties of rubber, *Proc R Soc Lond A Math Phys Sci* 274 (1356) (1963) 21–39.
- [26] N.K. Myshkin, M.I. Petrokovets, A.V. Kovalev, Tribology of polymers: adhesion, friction, wear, and mass-transfer, *Tribol. Int.* 38 (11–1) (2005–2006) 910–921.
- [27] B.N. J Persson, Theory of rubber friction and contact mechanics, *J. Chem. Phys.* 115 (8) (2001) 3840–3861.
- [28] S. Lafaye, C. Gauthier, R. Schirrer, Analysis of the apparent friction of polymeric surfaces, *J. Mater. Sci.* 41 (2006) 6441–6452.
- [29] H. Yoshizawa, J. Israelachvili, Fundamental mechanisms of interfacial friction. 2. Stick-slip friction of spherical and chain molecules, *J. Phys. Chem.* 97 (1993) 11300–11313.
- [30] A. Mondelin, F. Valiorgue, J. Rech, M. Coret, E. Feulvarch, Hybrid model for the prediction of residual stresses induced by 15-SPH steel turning, *Int. J. Mech. Sci.* 58 (2012) 69–85.
- [31] B.L. Tai, A.J. Jessop, D.A. Stephenson, A.J. Shih, Workpiece thermal distortion in minimum quantity lubrication deep hole drilling—finite element modeling and experimental validation, *J. Manuf. Sci. Eng.* 134 (1) (2012), 011008.
- [32] X. Yue, X. Yang, J. Tian, Z. He, Y. Fan, Thermal, mechanical and chemical material removal mechanism of carbon fiber reinforced polymers in electrical discharge machining, *Int. J. Mach. Tool Manufact.* 133 (2018) 4–17.
- [33] C.J. Roukema, Y. Altintas, Generalized modeling of drilling vibrations. Part I: time domain model of drilling kinematics, dynamics and hole formation, *Int. J. Mach. Tool Manufact.* 47 (2007) 1455–1473.
- [34] I. Lazoglu, G. Poulachon, C. Ramirez, M. Akmal, B. Marcon, F. Rossi, J.C. Outeiro, M. Krebs, Thermal analysis in Ti-6Al-4V drilling, *CIRP Annals* 66 (2017) 105–108.
- [35] R.S. Anand, K. Patra, Mechanistic cutting force modelling for micro-drilling of CFRP composite laminates, *CIRP Journal of Manufacturing Science and Technology* 16 (2017) 55–63.
- [36] Y. Karpat, O. Bahtiyar, B. Değer, B. Kaftanoglu, A mechanistic approach to investigate drilling of UD-CFRP laminates with PCD Drills, *CIRP Annals* 63 (2014) 81–84.
- [37] T. Augspurger, T. Berge, B. Döbbeler, Measurement and modeling of heat partitions and temperature fields in the workpiece for cutting Inconel 718, *AIISI 1045, Ti6Al4V, and AlMgSi0.5*, *J. Manuf. Sci. Eng.* 141 (2019), 061007-1.
- [38] S. Maegawa, Y. Morikawa, S. Hayakawa, F. Itoigawa, T. Nakamura, Mechanism for changes in cutting forces for down-milling of unidirectional carbon fiber reinforced polymer laminates: modeling and experimentation, *Int. J. Mach. Tool Manufact.* 100 (2016) 7–17.
- [39] C. Islam, I. Lazoglu, Y. Altıntaş, A three-dimensional transient thermal model for machining, *J. Manuf. Sci. Eng.* 138 (2016) (2016) 021003-1.
- [40] V. Kryzhanivskyy, V. Bushlya, O. Gutmichenko, R. M'Saoubi, J.-E. Ståhl, Heat flux in metal cutting: experiment, model, and comparative analysis, *Int. J. Mach. Tool Manufact.* 134 (2018) 81–97.
- [41] J.L. Merino-Pérez, R. Royer, E. Merson, A. Lockwood, S. Ayvar-Soberanis, M. B. Marshall, Influence of workpiece constituents and cutting speed on the cutting forces developed in the conventional drilling of CFRP composites, *Compos. Struct.* 140 (2016) 621–629.
- [42] N.E. Dowling, *Mechanical Behavior of Materials*, third ed., Pearson International, 2007.
- [43] A.X.H. Yong, G.D. Sims, S.J.P. Gnaniyah, S.L. Ogin, P.A. Smith, Heating rate effects on thermal analysis measurement of Tg in composite materials, *Adv. Manuf. Polym. Compos. Sci.* 3 (2) (2017) 43–51.
- [44] B.N.J. Persson, Rubber friction: role of the flash temperature, *J. Phys. Condens. Matter* 18 (2006) 7789–7823.
- [45] Y. Waddad, V. Magnier, P. Dufrenoy, G. De, Saxcé Heat partition and surface temperature in sliding contact systems of rough surfaces, *Int. J. Heat Mass Tran.* 137 (2019) 1167–1182.
- [46] T. Yashiro, T. Ogawa, H. Sasahara, Temperature measurement of cutting tool and machine surface layer in milling of CFRP, *Int Journal of Machine Tools and Manufacturing* 70 (2013) 63–69.
- [47] R. Joven, R. Das, A. Ahmed, P. Roobehjavan, B. Minaie, Thermal properties of carbon fiber/epoxy composites with different fabric weaves, in: *Proceedings of the 44<sup>th</sup> SAMPE International Symposium and Exhibition*, Charleston, SC, USA, 2012.